analytical chemistry

ARTICLE

pubs.acs.org/ac

Multianalyte On-Chip Native Western Blotting

Samuel Q. Tia,[‡] Mei He,[†] Dohyun Kim,[†] and Amy E. Herr*[,‡,†]

[†]Department of Bioengineering, University of California, Berkeley, 342 Stanley Hall, Berkeley, California 94720, United States

Supporting Information

ABSTRACT: We introduce and characterize multiplexed native Western blotting in an automated and unified microfluidic format. While slab gel Western blotting is slow and laborious, conventional multiplexed blotting ("reblotting": probing one sample with multiple antibodies) requires even more resources. Here we detail three key advances that enable an automated and rapid microfluidic alternative to slab gel reblotting. First, we introduce both assay and microdevice designs that integrate protein blotting against multiple antibody blotting regions with native polyacrylamide gel electrophoresis. This microfluidic integration strategy overcomes nonspecific material losses inherent to harsh antibody stripping steps typically needed for conventional reblotting; said conditions can severely limit analyte quantitation. Second, to inform rational design of the multiplexed microfluidic device we develop an analytical model for analyte capture on the blotting regions. Comparison to empirical observations is reported, with capture efficiencies of >85%. Third, we introduce label free detection that makes simultaneous and quantitative multiplexed measurements possible without the need for prelabeling of sample. Assay linear dynamic range spans 8−800 nM with assay completion in 5 min. Owing to the speed, automation, enhanced quantitation capability, and the difficulty of conventional slab gel Western reblotting, microfluidic multiplexed native Western blotting should find use in systems biology, in particular in analyses of protein isoforms and multimeric protein complexes.

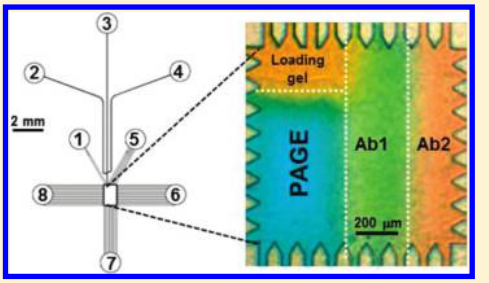

Western blotting is one of the most powerful and ubiquitous techniques for protein analysis. The multistage method integrates electrophoretic separations with subsequent immunoaffinity identification of targets, even for complex sample backgrounds.[1,2] However, preparation of a slab-gel immunoblot is laborious and time-consuming (~20 h) which can lead to workflow bottlenecks and high costs.[3] Further, the technique suffers from limited reproducibility and qualitative to semiquantitative performance.[4,5] Assays that require multistage workflows, such as Western blotting, have the potential to benefit tremendously from integration and automation.

Microsystems design enables unmatched capacity for lossless integration of functions, as well as ultralow sample volume consumption and efficient assay performance.[6,7] Recent promising assay design approaches have sought to integrate the functional advantages of microscale analysis with conventional macroscale components. For example, Ciaccio et al. report a technique for high throughput microwestern arrays in which microtiter-based liquid handling methods are used to print nanoliter arrays of cell lysate to a slab gel for semidry electrophoresis and blotting membrane transfer.[8] Anderson and coworkers demonstrate Western blotting within 1 h, using capillary electrophoresis with subsequent deposition of discrete protein zones to a poly(vinylidene difluoride) (PVDF) blotting membrane on a translational stage.[9] Similarly, Pan et al. have demonstrated Western blotting by performing microfluidic sodium dodecyl sulfate polyacrylamide gel electrophoresis (SDS-PAGE) within a poly(dimethylsiloxane) (PDMS) gasket which can then be mated to a PVDF membrane for traditional immunoblotting and enzymatic detection.[10]

In a purely microfluidic format, Native Western blotting was recently reported by our laboratory in a single microfluidic chip controlled by programmable voltage control.[11] The reported microfluidic design strategy sought to integrate advantages of fast, high-performance on-chip electrophoresis,[12−14] low-dispersion on-chip electrotransfer, and high capacity in-gel single analyte immunoassays to form a continuous workflow. While the assay reported charge-to-mass and immunoaffinity information quickly (<5 min), the approach was limited to measurement of a single analyte. Thus, commonly arising questions requiring multiplexed blotting (i.e., the study of relative protein expression levels or of subtypes and isoforms exhibiting different epitopes) from a single sample were not addressable with the reported assay. Conventional Western blotting of a single sample with subsequent blotting by multiple antibodies is known as reblotting.[15,16] Reblotting is frequently performed with nucleic acid assays (Southern and Northern blots)[17,18] but differences in antigen/antibody binding affinities and membrane adhesion make reblotting difficult for proteins (e.g., Western blots). One common approach to protein reblotting combines blotting with subsequent "stripping" steps which can require heat, extreme pH, and chaotropic agents to remove previously bound antibodies from the blotting membrane.[19] These

Received: February 7, 2011
Accepted: March 15, 2011
Published: April 01, 2011

harsh stripping steps often remove significant amounts of target protein and damage the blotting membranes, rendering quantitative comparisons of protein expression impossible.[20,21] This stripping limits the number of reblotting cycles as well as the multiplexed capability of the assay. Recycled membranes are not considered reliable for determination of protein absence and can only be used to confirm the presence of a protein.[22,23] Reprobing results in a considerable increase in assay time, as each step must be repeated—from washing and blocking to blotting, incubation, and detection. Alternative approaches to multitarget blotting are emerging,[24,25] yet challenges to interpretation arise if immunological reagents exhibit cross-reactivity or if multiple targets have similar electrophoretic mobility (e.g., protein isoforms).[26,27] Multiplexed immunoassays have been successfully demonstrated on-chip.[28−30] These multiplexed immunoassays (especially multispectral heterogeneous microfluidic immunoassays) yield high performance with fast read-outs and large multiplexing capabilities.

The present work seeks to surmount limitations of reblotting assays by harnessing the power of on-chip electrophoresis and the multiplexing capability of on-chip heterogeneous immunoassays to demonstrate the multiple steps comprising native Western reblotting—an assay advance important to systems biology and protein isoform analysis. To guide design of the multiplexed device and inform assay operation parameters, an analytical model for protein blotting during electrotransfer is developed and compared to empirical observations (e.g., analyte capture efficiency during electrotransfer). Finally, a label free technique is introduced with the integrated multistage format which eliminates sample prelabeling and allows quantitation of multiple protein targets simultaneously. In contrast to conventional reblotting, microfluidic reblotting obviates antibody stripping, detects target analytes in a single step, provides quantitative measurement, and completes in minutes.

EXPERIMENTAL SECTION

On-Chip Multianalyte Immunoblotting. The multiplexed immunoblotting assay is housed in a single 1 mm × 1.5 mm microchamber and microfluidic channel network (Figure 1a).[31] To fabricate the multiplexed blotting device, the microchamber is patterned with PA gel with specific regions for PAGE (loading and separation gels) and discrete antibody-patterned PA gel blotting "strips" that parallel the PAGE separation axis. To load the proteins into the central chamber, a ~2 μL sample volume is first pipetted into the sample reservoir (Figure 1a, reservoir 2). An electric potential maintained across reservoirs 2 and 4 results in protein loading across a standard injection t-junction. As depicted in Figure 1b, proteins are then electrophoretically injected and separated in a native PAGE region of the chamber. The separation region is comprised of a stacking interface (large-to-small pore size discontinuity, 3%T-to-6%T, w/v) and separation gel (6%T). As electrophoresis proceeds, proteins are resolved owing to differences in charge-to-mass ratio (Figure 1b, step 1). Control of voltages at electrodes 1 and 5 helps minimize sample dispersion and preserve high resolution analyte separation (see voltage program, Supporting Information Table S-1).[32−34] At separation completion, the separation electric field is removed and a lateral field is applied across the chamber, thus directing separated protein peaks to the antibody functionalized blotting regions (Figure1b, step 2). Each blotting region houses biotinylated capture antibody (specific to a protein target) linked to PA gel through a streptavidin-conjugated

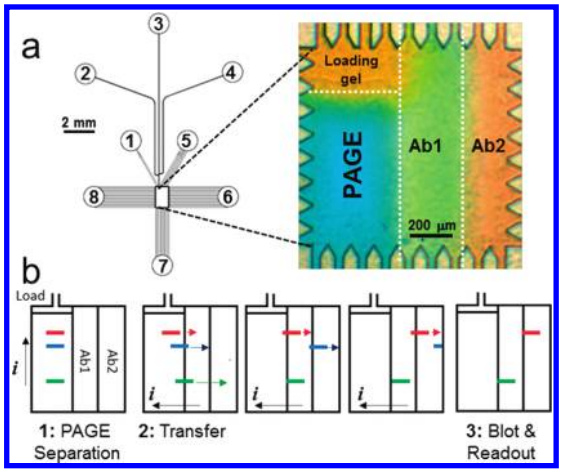

Figure 1. Multiplexed native Western reblotting integrated in a microfluidic device. (a) Microchannel and microchamber network design with fluid reservoirs numbered 1−8. A brightfield image of a chamber shows photopatterned gel regions: large pore-size loading gel, PAGE separation region, Ab1 and Ab2 discrete blotting regions. (b) Schematic of multianalyte blotting protocol. Step 1: PAGE separation resolves proteins along the separation axis, and current flow is indicated by "*i*". Step 2: lateral electrophoresis transfers resolved proteins to and through the blotting regions. Step 3: proteins bound to immobilized antibodies in each blotting region are retained, while all other species migrate out of the chamber.

acrylamide. Use of this adaptable linkage chemistry allows the blotting region to be customized with biotinylated antibodies prior to assay initiation.[35,36] As an example in Figure 1, two distinct blotting regions patterned with different antibodies (Ab1, Ab2) are shown.

As mentioned, the microchannel arrays bordering the central chamber maintain electric field uniformity along the separation and electrotransfer axes during PAGE separation and transfer, respectively.[37−39] The key performance metric for the transfer step is conservation of separation resolution (SR) from the separation axis to the blotting regions. A 1:1 spatial mapping of protein position on the separation axis to position on the blotting region is required to preserve critical charge-to-mass information. Thus, peak dispersion during electrotransfer must be minimized. In Figure 1b, step 3, proteins with an affinity for an immobilized antibody become immobilized as an immune-complex in the relevant blotting region. This in-gel binding process is somewhat analogous to that of 2D crossed electrophoresis, yet can be performed on a time scale of minutes (rather than hours).[40,41] Protein species with low-to-no affinity for the immobilized antibody migrate through and out of the blotting region without being retained. Detail on an analytical model and empirical results are described in the Results and Discussion section.

Reagents and Samples. Tris-glycine (25 mM Tris, 192 mM Glycine at pH 8.3) diluted to 1× was used as the sample and run buffer (Bio-Rad Laboratories, Hercules, CA). PA gels were prepared from a 30% acrylamide (29:1 acrylamide/bisacrylamide ratio) stock solution (Sigma-Aldrich, St. Louis, MO). Antibody functionalized blotting gels were prepared from a precursor solution which also contained streptavidin acrylamide (Invitrogen, Carlsbad, CA). All gel precursor solutions contained 0.2% (w/v) 2,2′-azobis-[2-methyl-*N*-(2-hydroxyethyl) propionamide] (VA-086) from Wako Chemicals (Richmond, VA) as a photoinitiator.

A fluorescently labeled protein ladder consisting of C-reactive protein (CRP) at 770 nM (EMD Chemicals Inc., Darmstadt,

Germany), protein G (PG) at 550 nM and trypsin inhibitor (TI) at 133 nM from Invitrogen was utilized for device and assay characterization. CRP was labeled in-house with AlexaFluor 488 (Invitrogen) according to manufacturer's instructions while PG and TI were purchased, already labeled by the vendor. Biotinylated anti-protein G (α-PG) antibodies were obtained from Abcam (Cambridge, MA) and biotinylated anti-CRP (α-CRP) was purchased from R&D Systems (Minneapolis, MN). Alternatively, antibodies can be conjugated using commercially available biotinylation kits (Thermo Scientific, Rockford, IL).

Multianalyte Blotting Chip Fabrication. Glass microfluidic chips were designed in-house with initial wet etching of glass conducted by the foundry at Caliper Life Sciences (Hopkinton, MA). The fluid access vias were drilled (Crystalite, Lewis Center, OH/Cameron Microdrill Presses, Sonora, CA) and chips were thermally bonded (Vulcan 3-550, Neytech, York, PA) in-house.[42] Prior to the introduction of gel precursor solutions, the glass chips were first incubated for 30 min with a 2:2:3:3 mixture of silane (3-(trimethoxysilyl) propyl methacrylate, Sigma-Aldrich), acetic acid, methanol, and water. This surface silanization step was critical to eliminating shifting of gel boundaries sometimes observed with extended application of an electric field (i.e., > 20 min) when silanization was not performed. After glass chip fabrication, three types of gels were fabricated in the 2D chamber: large pore-size loading gel (3%T, 3.3%C), smaller pore-size separation gel (6%T, 3.3%C), and antibody functionalized gel (4%T, 3.3%C containing 3.8 μM streptavidin-acrylamide) gels. Biotinylated antibodies were included at 1.6 μM in the blotting gel precursor solution and incubated for 1 h at room temperature (25 °C) prior to PA gel photopolymeriation.

Integration of discrete gel zones within a single device is enabled by the multistep photolithographic process detailed here in the Supporting Information (Figure S-1), which builds on a technique introduced in recent reports.[11,43] UV light is used to polymerize gel precursor solutions that are sequentially introduced into the central chamber. Importantly, this work expands single-analyte assay capabilities to multiplexed capabilities by taking advantage of high spatial resolution (~20 μm) photolithography techniques to enable more complex gel structures in the chamber. The multistep fabrication process yields a device with discrete loading and separation gel zones, as well as n blotting gel regions fabricated using $n + 2$ UV exposure steps (where n corresponds to the desired number of protein targets). Total fabrication time runs from 2 to 4 h depending on the experience of the operator and device complexity. Completed chips were stored for several weeks at 4 °C and fully submerged in an aqueous buffer solution. Although the blotting regions are designed for single use, the interior gels can be dissolved by immersing chips overnight in a perchloric acid (66%):hydrogen peroxide (33%) bath. Extreme care must be taken with this etching solution, as it is strongly caustic and can result in dangerous gas generation if containers are tightly capped (read relevant material safety data sheets (MSDSs)).

Fluidic Access and Voltage Control. To conduct the blotting assay, a photopatterned chip was seated on an epi-fluorescence microscope stage and ~2 μL of sample was aliquoted directly into the sample loading reservoir. All other reservoirs were loaded with Tris-glycine buffer, and a platinum electrode was inserted into each. Continuous control and monitoring of voltage and current levels at each electrode was accomplished using a custom built, eight channel high voltage power supply with current/voltage feedback control (Supporting Information Table S-1). Electrical field strengths within the device were estimated by dividing the difference in applied electrical potential by the distance between electrodes.

Data Collection and Analysis. Image collection was performed with a charge coupled device (CCD) camera (CoolSNAP HQ2, Roper Scientific, Trenton, NJ) and a 10× objective (UPlanFL, N.A. = 0.3, Olympus, Center Valley, PA) using an inverted epi-fluorescence microscope (IX-70, Olympus). Camera exposure time was 300 ms, and 2 × 2 pixel binning was employed, resulting in a full field image representing a ~1 mm × 1.34 mm field of view. Use of full field imaging allows all analytes to be simultaneously observed during protein separation and detected on antibody functionalized blotting regions after lateral transfer. Light from a mercury arc lamp was filtered through XF100-3 or XF111-2 filter sets (Omega Optical, Brattleboro, VT) for illumination of AlexaFluor 488 and 568 labeled proteins, respectively. Two color image composites were compiled from individual red and green wavelength image sequences taken during two independent, successive experimental realizations on the same device. Identical conditions and timing were maintained, and images from each color channel were synchronized to an electrical signal observed at the trigger of each experiment, then merged into a single sequence in postprocessing via ImageJ (NIH, Bethesda, MD).

Image analysis was performed using ImageJ and regions of interest (ROI) corresponding to the separation and blotting regions were selected and consistently applied. Line sections across the ROI were averaged to calculate the spatial distribution of the fluorescence signal. SR between protein bands is one of the most critical metrics of system performance, defined as $SR = \Delta L/4\sigma$, where ΔL is the distance between adjacent band centers and σ represents the average characteristic bandwidth (assuming Gaussian distribution).[44] Two analyte bands are resolved when SR > 1. σ was calculated by applying a Gaussian peak fitting algorithm using OriginPro (OriginLab, Northampton MA).

Simulation of Analyte Capture in Blotting Regions. Simulations were written and performed using Matlab (MathWorks, Natick MA).

RESULTS AND DISCUSSION

On-Chip Multiplexed Native Western Blot. To assess on-chip multiplexed reblotting performance and establish a robust assay protocol, the fluorescently labeled three analyte ladder was assayed. The ladder consisted of two target proteins (CRP, PG) and a high electrophoretic mobility negative control (TI). Results from the protein blotting assay are shown in Figure 2 with performance characterization of the three major steps (native PAGE separation, transfer, and multianalyte blotting) detailed in this section.

Native PAGE. To assess the injection dispersion minimization effect of the stacking gel, the standard deviation of the injected sample band was compared immediately before (σ_{inj}) and after passing through the stacking interface (σ_{stack}) within the microchamber. For the architecture used here, the presence of the stacking interface reduced injection dispersion by 75%, from σ_{inj} = 117 μm to σ_{stack} = 29 μm. Concomitantly, a 41% ± 19% (n = 6) increase in the maximum of the fluorescence signal was observed when a band crossed the stacking interface. Upon passing through the stacking interface (separation time of t = 17 s), the injected plug was resolved into PG (σ_{PG} = 122 μm), TI (σ_{TI} = 96 μm), and CRP (σ_{CRP} = 68 μm). At t = 17 s, all three species were baseline resolved, with an SR of 1.10 between TI/PG and 1.78 between PG/CRP. The separation (from stacking

gel to TI peak center) occupied 630 μm of the 1290 μm separation axis.

Electrophoretic Transfer to Blotting Regions. At t = 28 s, electrophoretic sample transfer from the native PAGE separation axis to the blotting regions was initiated. The separation electric field was switched off and an electric field was applied perpendicular to the separation axis to drive species across the separation chamber and to the blotting regions. Careful regulation of current flow at control reservoirs 1, 5, 6, 7, and 8 (Figure 1a) was employed to minimize fringing fields in the chamber, both during transfer (Figure 2b) and during the prior separation (see voltage control program for details, Supporting Information Table S-1).[32,34]

Full band transfer to the blotting regions was complete within 25 s for the PG peak (high mobility positive control) and within 210 s for the lower mobility CRP peak. The high mobility negative control migrated through both blotting regions and out of the 2D chamber within 50 s. The lateral electrotransfer was completed when the slowest species traversed the lateral span between the separation axis and last blotting region. Changes in protein bandwidth, peak positions, and SR before and after sample transfer and blotting are displayed in Table 1; note that control of band dispersion along the separation axis is critical for high resolution blotting. The average bandwidth decreases by an average of 16% (along the lateral dimension) after blotting, as compared to the width of the band during PAGE.

To assess nonspecific exclusion (e.g., physical size exclusion) or retention at the blotting gel interfaces (i.e., separation-to-blotting region, blotting region 1-to-2) and within each blotting region, negative control proteins not specific to the antibody functionalized gel were monitored. Supporting Information Figure S-2 further describes the transport of large negative control proteins (ranging from 66 to 150 kDa) which are able to pass through the blotting region. In the dual analyte assays, negligible change in electrophoretic mobility of the negative control protein (TI) was observed (μ_{TI} along separation axis: 4.93 × 10^{-5} $cm^2/(V\ s)$, μ_{TI} in α-CRP region: 4.93 × 10^{-5} $cm^2/(V\ s)$; μ_{TI} in α-PG region: 4.95 × 10^{-5} $cm^2/(V\ s)$). Negligible stacking and negligible destacking were observed at any gel interface in the lateral transfer direction (separation to blotting gel or between the two blotting regions) due to the closely matched pore-sizes both within the regions and at each lateral transfer interface.

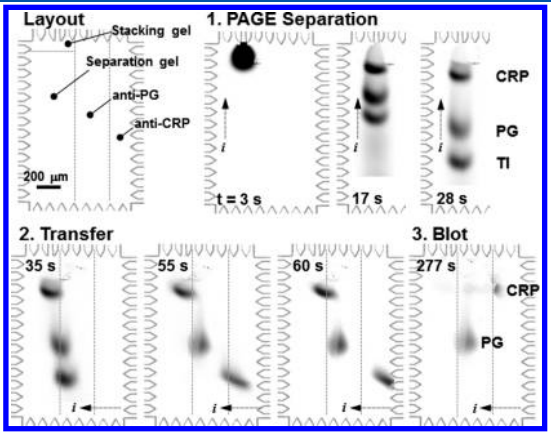

Figure 2. Discrete blotting regions enable (1) separation, (2) transfer, and (3) multiplexed blotting of unique targets from a single sample. Negative control (TI) shows no interaction with the blotting regions or interfaces. E = 95 V/cm during injection/separation, and E = 50 V/cm during transfer of separated proteins to the blotting regions (image collection via fluorescence microscopy).

Blotting and Fluorescence Readout. The dual analyte native blot yields a linear dose response from 8 to 800 nM ($y = 0.042x - 0.187$; $R^2 = 0.988$, measurements at 8, 50, 200, 400 and 800 nM), as measured via fluorescence imaging for the protein G sample. Plotting fluorescence intensity across the length of the protein band results in an area under the curve correlated to the total mass of protein capture. Comparisons of preblot and postblot PG and CRP band measurements demonstrate that between 85 and 95% of each protein band is captured on the matching antibody functionalized blotting regions. A lower limit of detection of 2.5 nM was established based upon a SNR of ~3 for the current standard epi-fluorescence based full field imaging system. The full field imaging capability was selected for use here, as it allows for simultaneous quantitative measurement of multiple analytes, so that sample band handling dispersion along both axes of the 2D chamber could be quantified at each time point. Subnanomolar levels of sensitivity are possible with more sensitive detection approaches, such as a scanning laser/photomultiplier tube system (and are currently under development for a high sensitivity version of the present assay).[45,46]

Establishing Conditions for Analyte Blotting. To establish optimal operating conditions for blotting, modeling of the immunoblotting process was performed. Assuming the interaction between migrating protein and immobilized antibody is sufficiently represented by a first order Langmuir binding model,[47] the concentration distributions of bound (C_{bound}) and free target protein (C) can be expressed as a binding reaction and a differential equation:

$$C + b_m \underset{k_{off}}{\overset{k_{on}}{\rightleftarrows}} C_{bound}$$

$$\frac{dC_{bound}}{dt} = k_{on} C(b_m - C_{bound}) - k_{off} C_{bound}$$

Table 1. Bandwidth, Peak Center Position, and Separation Resolution Maintained Throughout Lateral Transfer

analyte	bandwidth (μm)	variation	peak center shift[c] (μm)/% of separation axis	separation resolution $\Delta L/4\sigma$	variation
TI	127 (before[a])	3%	14/1%	TI/PG	18%
	123 (after[b])			1.26 (before)	
PG	171(before)	7%	29/2%	1.48 (after)	
	182 (after)			PG/CRP	6%
CRP	89 (before)	14%	53/4%	2.28 (before)	
	101 (after)			2.22 (after)	

[a] Imaged at 30 s. [b] Imaged at 250 s. [c] Peak center shift is defined as the net displacement of the peak center along the separation axis following lateral transport to the blotting region and is also represented in relative proportion to the length of the separation axis.

Here, b_m represents available binding sites on the immobilized antibody population. Free analyte binding at a binding site is governed by a forward association rate constant k_{on} (1/(M s)) and a backward dissociation rate constant k_{off} (1/s). For this system, the nondimensional Damköhler number (Da) represents the ratio of reactive flux (determined by k_{on} and availability of binding sites) to the mass transport flux (electromigration). Specifically, $Da = Lk_{on}b_m/U_o$ where L is the width of the blotting region and U_o represents the analyte electromigration speed through the blotting region.[48,49] Here, $U_o = \mu_o E$, where E is the applied lateral electric field strength and μ_o represents the electrophoretic mobility of the analyte, such that: $Da = Lk_{on}b_m/\mu_o E$. Thus, Da describes the relationship between two time scales: electromigration time ($L/\mu_o E$) and binding reaction time ($1/k_{on}b_m$). To provide context, when the value of Da is high (>10), the duration of protein target colocalization in the blotting gel significantly exceeds the characteristic time scale necessary for a binding reaction. Thus, the system is mass transport limited. At low Da (<1), the target moves through the blotting region too quickly for binding to occur and the system is reaction limited. Operating in the mass transport limited regime (Da > 10), while maintaining a reasonable total assay time as defined by the application, is desired.

Both the depletion of target band (ΔC_{bound}) and the spatial distribution of bound target within the blotting gel (C_{bound}) were modeled for a single target-band, single blotting-region system. Here, x corresponds to the lateral (transfer) axis of the microchamber. The migrating protein band was modeled in one dimension as a Gaussian distribution with width from -2σ to $+2\sigma$. The concentration distribution is divided into a series of n differential elements of equal width ΔX. Each band element is assigned an initial concentration value $C(x, t_o)$. The blotting region is similarly represented by p gel elements of equal width ΔX, such that $p = L/\Delta X$, where L represents the total length of the blotting region (Supporting Information Figure S-3).

Electrophoretic migration speed determines a residence time step (Δt) wherein each target band element is colocalized or "incubated" with a matching blotting gel element. The average peak migration speed through the blotting gel is assumed to be constant and uniform over all blotting regions. For each time step, the bound protein concentration is expressed by:

$$\Delta C_{bound} = (k_{on}C(b_m - C_{bound}) - k_{off}C_{bound})\Delta t$$

After each time step, the calculated ΔC_{bound} is adjusted to the corresponding band and gel elements. Note that time scales for k_{off} are typically 10^7-10^{10} larger than that of k_{on}.[50] In the simulation, the band is allowed to advance relative to the gel, and the next set of band/gel incubation steps is computed. Empirically determined electrophoretic mobility values and known sample/antibody concentrations were used (Table 2).

Selection of an appropriate k_{on} is critical in fitting the model, as k_{on} is the only parameter which cannot be directly extracted from empirical observation and system design. Values for k_{on} can vary by several orders of magnitude depending upon the antigen/antibody pair and local microenvironment.[51,52] While the present model does not capture the full convection-diffusion behavior of the band, band migration through the blotting region is relatively short when compared to the transfer and separation period, thus substantiating neglect of diffusive effects in the blotting gel during binding interactions. Figure 3 compares results obtained from simulation to experimental results in which an 800 nM PG sample was transferred to an α-PG blotting gel at

Table 2. Simulation Parameters, Both Empirical and a priori Determined

variable [units]	relevant parameter range	experimental	simulation
b_m [μM][49]	0−22	1.6*	1.6
E [V/cm]	10 −150	30−110	14−140
L [μm]	20−500	100−300	100−200
k_{on} [1/(M s)][50,51]	10^4-10^8		5.75×10^5
k_{off} [1/s][51,52]	$10^{-1}-10^{-5}$		1×10^{-3}
μ_o [cm^2/(V s)][53]	$1-7 \times 10^{-5}$	6.6×10^{-5}	6.6×10^{-5}
σ [μm]	10−100	80	80
C [nM][54,55]	1−500	8−1250	800

* Assuming full binding site availability.

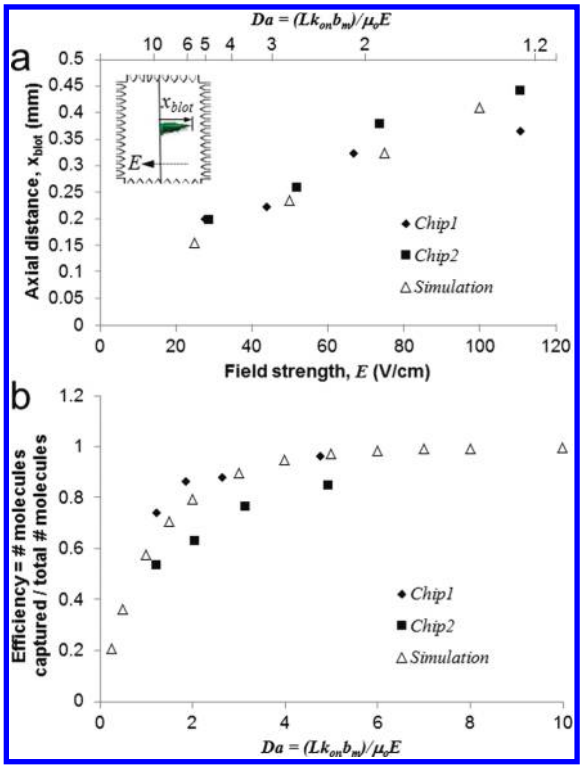

Figure 3. Modeling of binding in blotting regions informs selection of electrotransfer conditions to maximize binding efficiency. (a) Band distribution as a function of lateral field strength, experimental results vs simulation. (b) For a given chip geometry (blotting region width and binding site density), target capture efficiency varies as a function of Da.

specified lateral field strengths. Here, the length of the immobilized band is defined as the distance from the separation/blotting gel interface that contains 90% of the total area-under-curve when bound antigen concentration is plotted as a function of space. In simulation and in experimental work, the length of the blotting region required for full antigen capture increases linearly as a function of applied field strength. A 500 μm lateral distance is sufficient for total capture of this antigen—even for a high concentration target in lateral fields of greater than 100 V/cm (Figure 3a).

Figure 3b illustrates how variations in binding efficiency are influenced by parameters such as field strength and sample properties. Assuming a blotting region width of 100 μm and a binding site density of 1.6 μM, the values for E are varied from

14 to 140 V/cm, μ_o is varied from 2×10^{-5} to 40×10^{-5} $cm^2/(V\ s)$, and k_{on} is varied from 0.5×10^5 to 20×10^5 $1/(M\ s)$. Binding efficiency is used as a metric of target capture. If the width of the blotting region is less than the requisite dimensions of the full immobilized band, the efficiency of protein capture will be suboptimal. Alternatively, if the width of the blotting region is substantially more than needed, the multiplexed capability of this reblotting assay would be unnecessarily reduced.

The model detailed here is useful for optimizing performance and informing device design. Knowledge of the minimum blotting gel width for a specific set of operating (i.e., E, L) and analyte characteristics (i.e., antigen/antibody binding affinities, analyte mobility) is especially helpful in maximizing the capacity of a multianalyte blotting assay. Upon the basis of the requisite lengths of the lateral transfer regions under current conditions, it is estimated that blotting against 8−10 antibodies is feasible with further expansion of the central chamber. Specifically, the model aids in device design for biological applications where the electrophoretic mobility and binding affinity constants may range widely for species in one multianalyte sample. When experimental results are compared against simulations, the spatial distribution of an immobilized band can also serve as a basis for estimating previously unknown binding affinities.[56]

In many cases it may be advantageous to lower the strength of the lateral electric field, thus prolonging the time in which the antigen target is colocalized to the capture antibody during sample transfer. This increased "incubation time" results in a higher capture efficiency and enhances the localized blotting signal which determines the limit of detection.[57] However, a slower transfer speed could also result in greater diffusive band dispersion. Alternatively, one could increase the local capture antibody concentration to minimize the requisite lateral trapping length and increase measurement sensitivity. On-chip arrangement of various antibody functionalized regions can be customized depending upon the transfer behavior of the analytes. For example, cross reactivity between antibodies for multiple species within a single sample can often present an obstacle to all forms of immunoassay. In cases where known cross reactivity exists between binding antigen/antibody pairs, the sequence of antibody functionalized blotting regions within a 2D chip can be specified to minimize ambiguous or spurious measurements. Note that blotting region widths need not be identical for all target species.

Blotting of Comigrating Species As Relevant to Analysis of Protein Isoforms. In conventional blotting assays, stripping and reblotting of the blotting membranes (i.e., PVDF or nitrocellulose sheet) may be the only option when two antigens exhibit closely matched electrophoretic velocities. This is especially true in studies of isoforms or post-translational modifications of a protein which result in relatively small differences in molecular weight. On-chip blotting was assessed as a means to selectively blot and identify one of two comigrating species from native PAGE. Two-color imaging data presented in Figure 4 shows native PAGE analysis of a sample comprised of fluorescently labeled PG target (red fluorescent label) and a sample ladder composed of BSA and TI (green fluorescent label). The PG band displayed an electrophoretic velocity which differs by 10% from BSA, thus species comigrate early in the native PAGE assay.

At an elapsed PAGE separation time of $t = 27$ s, the electric field was switched to the lateral direction and all species migrated to the blotting region located at chamber right. Transfer at 50 V/cm required 38 s. Upon blotting against an α-PG antibody immobilized in the blotting region, the red-labeled PG was specifically

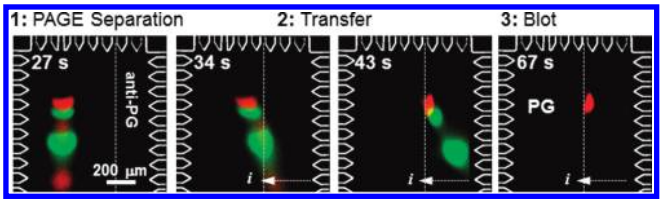

Figure 4. Protein immunoblotting enables selective protein blotting for comigrating species. Two color image composite shows native PAGE (27 s) with two comigrating species, here red labeled protein G and green labeled BSA. Green labeled TI acts as a fast moving negative control. The fastest red peak is free dye. Lateral transfer moves all species to the single blotting region (34 and 43 s), housing immobilized antibodies against protein G. Red labeled protein G is selectively bound while both BSA and TI migrate out of the chamber (67 s).

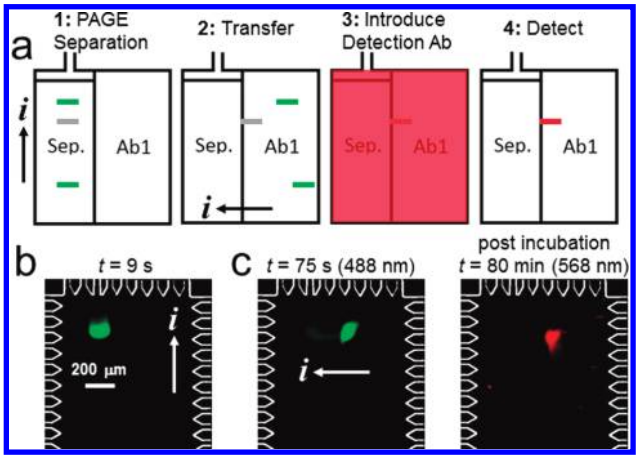

Figure 5. Sandwich assay allows for detection of an unlabeled sample (SNR ~38). (a) Illustration of on-chip technique for resolution and detection of an unlabeled sample. (b and c) The AF488 (green) labeled immobilized protein target is visible under green fluorescence excitation; it is initially invisible at the red wavelength until it is incubated with Texas Red labeled primary antibody.

retained in the α-PG blotting region. Binding efficiency, defined as *# molecules bound/total # molecules* (based upon fluorescence intensity measurement), is estimated at 95% for PG. All nontarget bands migrated through the blotting region ($t = 30$−65 s) with no detectable fluorescent signal, leaving behind the captured antigen of interest. The immunoblot was completed 65 s after sample injection.

Label Free Detection on the Blotting Regions. To yield label free on-chip native Western blotting, all assay steps proceeded as described earlier in this study with exceptions being (1) the protein sample was no longer fluorescently labeled prior to PAGE and (2) a fluorescently labeled detection antibody was introduced after analyte capture on the blotting region. Here, the assay was demonstrated for PG at 500 nM. To more clearly illustrate the assay concept, PG was labeled with a green fluorophore (detection antibody is labeled with red). In practice, the sample proteins would not be labeled but a dye-labeled protein ladder could be included with the sample as a relative mobility reference. After sample capture, fluorescently labeled detection antibody (6 μM) matched to the blotted target was introduced to the blotting region from the control channel array at device right (E = 150 V/cm). The detection antibody was then electrophoretically flushed out of the blotting/separation

chamber after a 20 min incubation period. (Optimization of incubation time is currently underway and dependent on the analyte and detection antibody.) As observed in Figure 5, the detection antibody reported a fluorescence signal (red, SNR ~ 39) at the position of the immobilized target protein band on the blotting region (as illustrated in green). The approach is also compatible with enzyme-linked amplification to further enhance the detection signal upon the blotting region.[58,59]

SUMMARY AND CONCLUSIONS

We have introduced, fabricated, and characterized an integrated assay that reports (1) analyte electrophoretic mobility obtained via native PAGE with (2) subsequent antibody-based blotting of multiple species. We detail contributions that include a microfluidic framework for automated operation of reblotting assays suitable for analyte quantitation. The microfluidic format surmounts notable challenges which limit the use of reblotting in slab gels. Further, we develop an analytical model that captures the competition between analyte electromigration and affinity based analyte capture in a gel blotting region. The model was used to inform device design (e.g., lateral dimension of blotting regions and the maximum number of feasible blotting regions for the geometry described here) and selection of assay operating conditions (e.g., electrotransfer field strength) for optimum protein binding efficiency. Lastly, we detail a multistage sample and reagent delivery functionality which underpins a label free assay strategy that uses a sandwich antibody detection approach. Multispectral detection and enzyme amplification can be employed to expand the analytical capacity of the assay in terms of multiplexing and analytical sensitivity, respectively. Both added functionalities are currently under development. The multiplexed immunoblotting technology developed here for native protein analysis was demonstrated for both well resolved and unresolved proteins (from PAGE) and yielded total automated assay completion on the order of minutes (a time savings of several orders of magnitude). Given the appreciable throughput (assay speed, multiplexing capability) and the detection functionalities demonstrated, this assay may comprise part of a tool set necessary to advance toward high throughput proteomics and enhance systems biology based inquiry.

ASSOCIATED CONTENT

Supporting Information. Figures illustrating multistep photolithography process, comparison of blotting results from positive and negative control experiments as well as details regarding custom voltage control hardware, and sample voltage program. This material is available free of charge via the Internet at http://pubs.acs.org

AUTHOR INFORMATION

Corresponding Author

*E-mail: aeh@berkeley.edu. Tel.: +1 510 666 3396.

Notes

‡The UC Berkeley−UCSF Graduate Program in Bioengineering.

ACKNOWLEDGMENT

The authors thank Gautham Venugopalan (Fletcher Lab, UC Berkeley) for assistance. The authors gratefully acknowledge the University of California, Berkeley, and the QB3/Rogers Family Foundation Award for financial support. This work also supported by the National Institutes of Health through the NIH Director's New Innovator Award Program (A.E.H., 1DP2OD007294). Infrastructure support was provided by the QB3 Biomolecular Nanofabrication Center (Stanley Hall, UC Berkeley campus). S.Q.T. is a National Science Foundation Graduate Research Fellow. A.E.H. is an Alfred P. Sloan Foundation Research Fellow in chemistry.

REFERENCES

(1) Towbin, H.; Staehelin, T.; Gordon, J. *Proc. Natl. Acad. Sci. USA* **1979**, *76*, 4350–4354.
(2) Westermeier, R.; Marouga, R. *Biosci. Rep.* **2005**, *25*, 19–32.
(3) Alegria-Schaffer, A.; Lodge, A.; Vattem, K. *Methods Enzymol.* **2009**, *463*, 573–599.
(4) Fido, R. J.; Tatham, A. S.; Shewry, P. R. *Methods Mol. Biol.* **1995**, *49*, 423–437.
(5) Tovey, E. R.; Baldo, B. A. *J. Biochem. Biophys. Methods* **1989**, *19*, 169–183.
(6) Folch, A. *J. Vis. Exp.* **2007**, 300.
(7) Gourley, P. L. *Biotechnol. Prog.* **2005**, *21*, 2–10.
(8) Ciaccio, M. F.; Wagner, J. P.; Chuu, C. P.; Lauffenburger, D. A.; Jones, R. B. *Nat. Methods* **2010**, *7*, 148–155.
(9) Anderson, G. J.; C, M. C.; Kennedy, R. T. *Anal. Chem.* **2011**, *83*, 1350–1355.
(10) Pan, W.; Chen, W.; Jiang, X. *Anal. Chem.* **2010**, *82*, 3974–3976.
(11) He, M.; Herr, A. E. *J. Am. Chem. Soc.* **2010**, *132*, 2512–2513.
(12) Hatch, A. V.; Herr, A. E.; Throckmorton, D. J.; Brennan, J. S.; Singh, A. K. *Anal. Chem.* **2006**, *78*, 4976–4984.
(13) Yang, S.; Liu, J.; DeVoe, D. L. *Lab Chip* **2008**, *8*, 1145–1152.
(14) Yao, S.; Anex, D. S.; Caldwell, W. B.; Arnold, D. W.; Smith, K. B.; Schultz, P. G. *Proc. Natl. Acad. Sci. USA* **1999**, *96*, 5372–5377.
(15) Chen, D.; Chen, S.; Wang, W.; Liu, F.; Zhang, C.; Zheng, H. *Acta Otolaryngol.* **2010**, *130*, 1411–1420.
(16) Guther, M. L.; de Almeida, M. L.; Rosenberry, T. L.; Ferguson, M. A. *Anal. Biochem.* **1994**, *219*, 249–255.
(17) Keane, B.; Lim, H. W.; Rogstad, S. H. *Plant Mol. Bio. Report* **2000**, *18*, 17–21.
(18) Yang, H.; McLeese, J.; Weisbart, M.; Dionne, J. L.; Lemaire, I.; Aubin, R. A. *Nucleic Acids Res.* **1993**, *21*, 3337–3338.
(19) Kaufmann, S. H.; Ewing, C. M.; Shaper, J. H. *Anal. Biochem.* **1987**, *161*, 89–95.
(20) Gallagher, S.; Winston, S. E.; Fuller, S. A.; Hurrell, J. G. *Current Protocol in Immunology*, Colligan, J. E., Ed.; Wiley-Interscience: New York, 2008; Vol. 83, 8.10.1−8.10.28.
(21) Sennepin, A. D.; Charpentier, S.; Normand, T.; Sarre, C.; Legrand, A.; Mollet, L. M. *Anal. Biochem.* **2009**, *393*, 129–131.
(22) Krajewski, S.; Huang, X.; Krajewska, M. *Methods Mol. Biol.* **2009**, *536*, 473–481.
(23) Kurien, B. T.; Scofield, R. H. *Methods Mol. Biol.* **2009**, *536*, 557–571.
(24) Gingrich, J. C.; Davis, D. R.; Nguyen, Q. *Biotechniques* **2000**, *29*, 636–642.
(25) Krajewski, S.; Zapata, J. M.; Reed, J. C. *Anal. Biochem.* **1996**, *236*, 221–228.
(26) Kaufmann, S. H. In *The Protein Protocols Handbook*, Third ed.; Walker, J. M., Ed.; Humana Press: Totowa, NJ, 2009; pp 789−806.
(27) Laycock, C. A.; Phelan, M. J.; Bucknall, R. C.; Coleman, J. W. *Ann. Rheum. Dis.* **1994**, *53*, 256–260.
(28) Kartalov, E. P.; Zhong, J. F.; Scherer, A.; Quake, S. R.; Taylor, C. R.; Anderson, W. F. *Biotechniques* **2006**, *40*, 85–90.
(29) Liu, J.; Chen, C. F.; Chang, C. W.; DeVoe, D. L. *Biosens. Bioelectron.* **2010**, *26*, 182–188.
(30) Fan, R.; Vermesh, O.; Srivastava, A.; Yen, B. K.; Qin, L.; Ahmad, H.; Kwong, G. A.; Liu, C. C.; Gould, J.; Hood, L.; Heath, J. R. *Nat. Biotechnol.* **2008**, *26*, 1373–1378.

(31) He, M.; Herr, A. E. *Anal. Chem.* **2009**, *81*, 8177–8184.
(32) Lerch, M. A.; Hoffman, M. D.; Jacobson, S. C. *Lab Chip* **2008**, *8*, 316–322.
(33) Han, J.; Craighead, H. G. *Science* **2000**, *288*, 1026–1029.
(34) Lerch, M. A.; Jacobson, S. C. *Anal. Chem.* **2007**, *79*, 7485–7491.
(35) Lesch, H. P.; Kaikkonen, M. U.; Pikkarainen, J. T.; Yla-Herttuala, S. *Expert Opin. Drug Deliv.* **2010**, *7*, 551–564.
(36) Rusmini, F.; Zhong, Z.; Feijen, J. *Biomacromolecules* **2007**, *8*, 1775–1789.
(37) Bakajin, O.; Duke, T. A.; Tegenfeldt, J.; Chou, C. F.; Chan, S. S.; Austin, R. H.; Cox, E. C. *Anal. Chem.* **2001**, *73*, 6053–6056.
(38) Lin, R.; Burke, D. T.; Burns, M. A. *Anal. Chem.* **2005**, *77*, 4338–4347.
(39) Huang, L. R.; Tegenfeldt, J. O.; Kraeft, J. J.; Sturm, J. C.; Austin, R. H.; Cox, E. C. *Nat. Biotechnol.* **2002**, *20*, 1048–1051.
(40) Emmett, M.; Crowle, A. J. *J. Immunol. Methods* **1982**, *50*, R65–83.
(41) Laine, A.; Ducourouble, M. P.; Hannothiaux, M. H. *Anal. Biochem.* **1987**, *161*, 39–44.
(42) Harrison, D. J.; Fluri, K.; Seiler, K.; Fan, Z.; Effenhauser, C. S.; Manz, A. *Science* **1993**, *261*, 895–897.
(43) He, M.; Herr, A. E. *Nat. Protoc.* **2010**, *5*, 1844–1856.
(44) Giddings, J. C. *Unified Separation Science*; Wiley-Interscience: New York, 1991.
(45) Chou, H. P.; Spence, C.; Scherer, A.; Quake, S. *Proc. Natl. Acad. Sci. USA* **1999**, *96*, 11–13.
(46) Dishinger, J. F.; Kennedy, R. T. *Electrophoresis* **2008**, *29*, 3296–3305.
(47) Sadana, A.; Vo-Dinh, T. *Appl. Biochem. Biotechnol.* **1997**, *67*, 1–22.
(48) Bharadwaj, R.; Park, C. C.; Kazakova, I.; Xu, H.; Paschkewitz, J. S. *Anal. Chem.* **2008**, *80*, 129–134.
(49) Squires, T. M.; Messinger, R. J.; Manalis, S. R. *Nat. Biotechnol.* **2008**, *26*, 417–426.
(50) Hu, G.; Gao, Y.; Li, D. *Biosens. Bioelectron.* **2007**, *22*, 1403–1409.
(51) Schuck, P. *Curr. Opin. Biotechnol.* **1997**, *8*, 498–502.
(52) Zhuang, G.; Katakura, Y.; Omasa, T.; Kishimoto, M.; Suga, K. *J. Biosci. Bioeng.* **2001**, *92*, 330–336.
(53) Herr, A. E.; Singh, A. K. *Anal. Chem.* **2004**, *76*, 4727–4733.
(54) Don, B. R.; Kaysen, G. *Semin. Dial.* **2004**, *17*, 432–437.
(55) Wadsworth, G. R.; Oliveiro, C. J. *Br. Med. J.* **1953**, *2*, 1138–1139.
(56) Wei, Y.; Wesson, P. J.; Kourkine, I.; Grzybowski, B. A. *Anal. Chem.* **2010**, *82*, 8780–8784.
(57) Buchanan, D. D.; Jameson, E. E.; Perlette, J.; Malik, A.; Kennedy, R. T. *Electrophoresis* **2003**, *24*, 1375–1382.
(58) Bratthauer, G. L. *Methods Mol. Biol.* **2009**, *588*, 231–241.
(59) Marquette, C. A.; Blum, L. J. *Anal. Bioanal. Chem.* **2008**, *390*, 155–168.